NETWORKS AND HETEROGENEOUS MEDIA
©American Institute of Mathematical Sciences
Volume **2**, Number **2**, June **2007**
Website: http://aimSciences.org
pp. **211–225**

A NEW MODEL FOR CONTACT ANGLE HYSTERESIS

Antonio DeSimone*, Natalie Grunewald† and Felix Otto†

*SISSA-International School for Advanced Studies
Via Beirut 2-4, 34014, Trieste, Italy

†Institut für Angewandte Mathematik
Wegelerstr. 10, 53115, Bonn, Germany

(Communicated by Benedetto Piccoli)

Abstract. We present a model which explains several experimental observations relating contact angle hysteresis with surface roughness. The model is based on the balance between released capillary energy and dissipation associated with motion of the contact line: it describes the stick–slip behavior of drops on a rough surface using ideas similar to those employed in dry friction, elasto–plasticity and fracture mechanics. The main results of our analysis are formulas giving the interval of stable contact angles as a function of the surface roughness. These formulas show that the difference between advancing and receding angles is much larger for a drop in complete contact with the substrate (Wenzel drop) than for one whose cavities are filled with air (Cassie-Baxter drop). This fact is used as the key tool to interpret the experimental evidence.

1. **Introduction.** We consider liquid drops resting on a rough solid surface. The angle at which the liquid/vapor interface meets the solid is the contact angle. While Young's law gives *one* value of this angle, the one associated with a drop minimizing the total interfacial energy, contact angle hysteresis shows that there exists a whole interval of stable contact angles. Both the end points and the width of this interval depend in a non–monotone way on the roughness of the solid, see the reviews [5], [17], and [6]. Figure 1, taken from [7], shows some well known measurements of advancing and receding angles which bound the interval of stable contact angles (the *hysteresis interval*).

More recent experiments show that, even at constant roughness, there may be more than one value for the receding angle, depending on the details of the drop deposition process, see [11]. In fact, in Figure 2, a large pressure is exerted on a Cassie–Baxter (CB) drop (i.e., a drop which has vapor-filled cavities underneath) which turns it into a Wenzel (W) drop (i.e., a drop with complete contact with the underlying surface) inducing a dramatic change in the measured receding angle. Another recent observation is that plants use roughness to make the surfaces of their leaves ultrahydrophobic, see [3], although their constitutive material might in principle even be hydrophilic. A mechanism by which roughness may lead to CB–drops with large contact angles on hydrophilic surfaces, in spite of their high cost in terms of surface energy, is discussed in [10].

We introduce a new model to capture these phenomena. It predicts a much narrower hysteresis interval for CB–drops than for W–drops. This can explain both the downward jump at large pressures of the experimental points in Figure 2,

2000 *Mathematics Subject Classification.* Primary: 76B45, 49S05; Secondary: 74C05.
Key words and phrases. Surface tension and related phenomena, Wetting, Drops and bubbles.

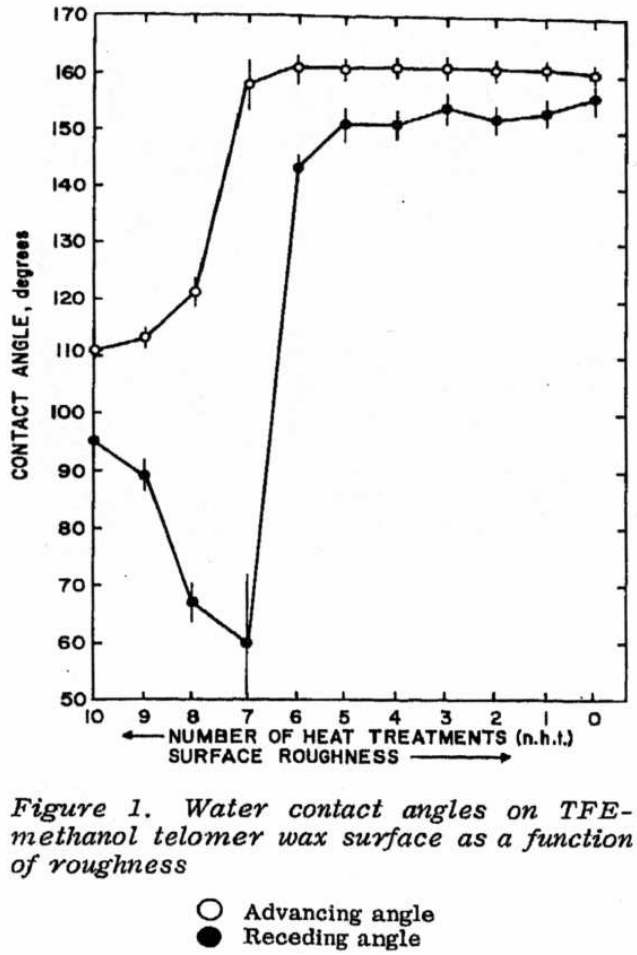

FIGURE 1. Experimental dependence of advancing and receding contact angles on the surface roughness. Reprinted with permission from [7]. Copyright (1964) American Chemical Society

and the non–monotone behavior of Figure 1. The main result of this paper is the quantitative dependence of the hysteresis interval on the surface roughness and the type of drop. It is given both in terms of formulas (see Equations (3.2)–(3.4)) and in terms of stability diagrams (see Figures 7–9).

Our model also leaves the possibility of metastable drops. That is, drops can be stable without minimizing surface energy. In fact, CB–drops can even be stable on hydrophilic surfaces and exhibit on them the large contact angles typical of super–hydrophobicity.

Our new model shares with similar ones used in dry friction [15], fracture and damage mechanics [8], [9], and elasto–plasticity [4] two main features. First, there is a critical "loading" that needs to be overcome before the system starts to dissipate energy. In our case, adding liquid to an existing stable drop at first only changes the contact angle and the drop does not move. Surface energy is only dissipated after

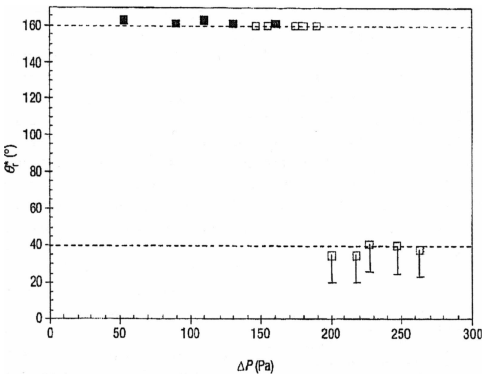

FIGURE 2. Experimental dependence of receding contact angles on the pressure pushing the drop onto the surface. Drops are of CB–type at low pressure and of W–type at high pressure. Reprinted from [11] with permission.

the drop starts moving. Second, the model is rate independent, i.e., the response of the system does not depend on the loading rate. Loading the system at a doubled rate will lead to the same response, at twice the speed.

The main idea behind our model is that the stability of a drop is not related to global or local minimality of its interfacial energy, but rather to the fact that the energy–landscape seen by a stable drop should not be too steep. More precisely: if the energy that would be gained by moving (i.e., the slope of the energy landscape) is smaller than the energy that would be dissipated through the motion, then the drop will not move. Once the drop starts moving, the dynamics is controlled by the balance between available energy and energy dissipated through motion. Of course, we are here focusing on the quasi-static limit (no inertia) and on small drops (no gravity, and viscous dissipation inside the drop negligible with respect to dissipation at the moving contact line). On the other hand, we assume that the size of the asperities is much smaller than the size of the drops. In order to implement these ideas, we use the derivative–free framework proposed in [13] (see also the review [14]).

Our model implies four different diagrams of stable contact angles, depending on the type of drop (W– or CB–type) and on the state of the surface in the vicinity of the contact line (dry or with puddles). It turns out that CB–drops are never stable when surrounded by water-filled cavities, while the three nontrivial diagrams are shown in Figures 7–9.

The model can also predict the time evolution under slowly changing external loads (e.g. the adding or removing of liquid). It identifies the microstructure (i.e., the microscopic pattern of contacts) with which the drop will advance or recede, which corresponds to the most unstable direction in the given energy landscape.

Our approach gives a qualitative explanation of the experiments mentioned above. Figure 1 can be understood as a superposition of the two stability diagrams for a dry surface. The highly non–monotone behavior of the width of the hysteresis interval comes from a transition from W–drops (Figure 7) to CB–drops (Figure 8). Indeed, using a notion of stability introduced in Section 3.2, one can show that, for the case of a dry surface, the stable configurations at low roughness are of W–type.

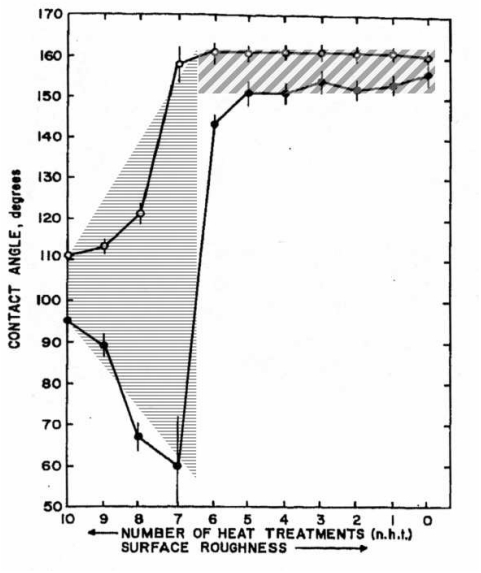

FIGURE 3. Stable contact angles according to our model (shaded regions; schematic plot), superposed on the experimental data from Figure 1.

At higher roughness, the stable configurations are instead CB , see Figure 10, and they display a much narrower hysteresis interval.

The stable contact angles resulting from the transition from W– to CB–drops are shown schematically in Figure 3, where they are superposed on the experimental results of Johnson and Dettre. The comparison is only qualitative, because in the experimental data roughness is measured only indirectly, through the number of heat treatments undergone by the solid surface in the sample preparation. The figure shows a transition from a regime in which the difference between advancing and receding contact angles increases monotonically with roughness, to one in which such a difference is smaller, and insensitive to roughness. At least in the two-dimensional geometry analyzed in the paper, the difference between the cosines of advancing and receding contact angles turns out to depend linearly on the area of solid tops, see the discussion in Section 3. A more stringent test of our model against experimental evidence would be desirable: such a comparison is indeed feasible, given the reliability with which artificial surfaces can be manufactured today matching a prescribed topographic pattern.

Figure 2 reflects the fact that the stability interval depends on the type of drop. Assuming that the corresponding surface is dry and has sufficiently large roughness ($r > r^*$ in the notation of Section 3), we see from Figures 7 and 8 that forcing a transition from a CB to W drop (by applying a large enough pressure) may reduce the lower end of the stability interval (i.e., the receding contact angle) from well above to well below 90°.

Our model can also reproduce the arguments in [10] in so far that CB–drops can be stable on a hydrophilic surface, although they do not minimize surface energy, see Figure 11.

The rest of the paper is organized as follows. In Section 2, we describe the model in detail. In Sections 3 and 4, our results and their physical implications are discussed without proofs. These are deferred to Section 5.

2. **A new model for contact angle hysteresis.**

2.1. **Setup and notation.** In the following we assume a 2–d setup, i.e., both surface and drops are infinitely extended along one direction (perpendicular to the plane of Figure 4). Although this assumption is not necessarily valid in experiments, see [5], it is very useful in a first attempt to build some intuition.

The solid surface is described by a periodic step function $S : [-R, R] \to (-\infty, 0]$ for some sufficiently large $R \in \mathbb{R}_+$. Here $S(x)$ is the height of the solid at position $x \in [-R, R]$. The two relevant parameters for S are its roughness r (i.e. the length of the surface divided by the length of its horizontal projection) and its proportion of tops $\varphi < 1$ (i.e., the ratio between the length of the solid tops within a unit cell, and the length of the horizontal projection of the unit cell), see Figure 4. It is normalized in such a way that at the tops $S(x) = 0$, and its period is of length $\varepsilon \ll 1$.

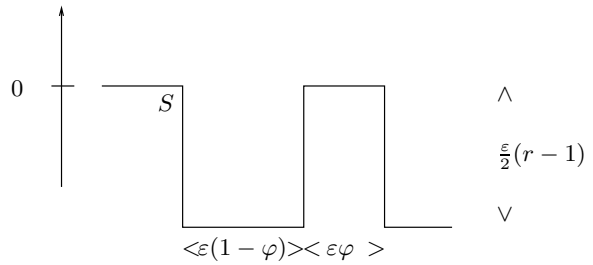

FIGURE 4. Microscopic roughness of the solid

This gives a generic surface, for which the area of contact with a drop can be easily determined: It is either the whole surface, or the tops without the cavities. This is a simplification with respect to smooth surfaces for which the wetted area needs to be computed by finding configurations meeting the wall cavities at the right microscopic contact angles. In this case, the proportion of wetted area φ does depend on the exact shape of the surface. This, however, does not introduce new features to the model: it will lead to the same results, but with a variable φ.

Furthermore, we introduce a region near the solid: $RS := \{(x, y) \,|\, x \in [-R, R]\,,\, y \in [S(x), 0]\}$, see Figure 5, and the box: $B := [-R, R] \times (0, 1]$. Note that the height of B can be chosen arbitrarily as long as it is much bigger than the periodicity of the microstructure of the solid (i. e. $\varepsilon \ll 1$). At time t a drop is given by some subset $L(t) \subset \{B \cup RS\}$, where the liquid is located. A time dependent drop configuration is described by the function L from $[0, \infty)$ into the subsets of $\{B \cup RS\}$.

We restrict our attention to drops which are of the following form (see Figure 5): The liquid is situated at the left side of $\{B \cup RS\}$. Inside B the boundary of $L(t)$ forms a liquid/vapor interface which consists of a straight line. This line meets the solid at position $X(L(t))$ and the upper boundary of B at position $Z(L(t))$. We call $X(L(t))$ the triple point and $Z(L(t))$ the upper interface point. The angle formed between the boundary of B and the liquid/vapour interface at position $Z(L(t))$ is the contact angle $\theta(L(t))$. In the region near the solid, $L(t)$ can have two possible

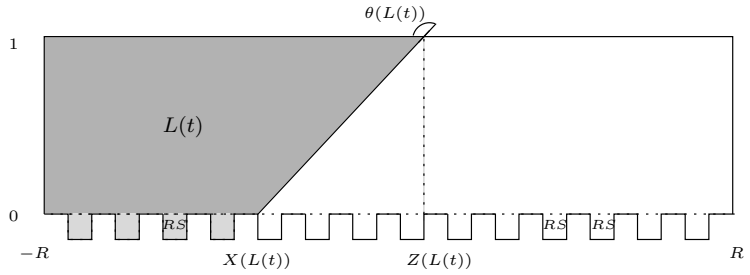

FIGURE 5. Drop configuration

configurations: either W–type (the cavities $\{RS|_{x<X(L(t))}\}$ are all nonempty) or CB–type (the cavities $\{RS|_{x<X(L(t))}\}$ are all empty). The discussion at the end of Section 2.3 shows that we only need to consider configurations whose L/V–interfaces are straight lines. Also drops with half filled cavities will not give new insight.

The boundary of $L(t)$ at the solid forms the solid/liquid interface $\Sigma_{S/L}$. The rest of S is the solid/vapour interface $\Sigma_{S/V}$. And the rest of the boundary of $L(t)$ is the liquid/vapour interface $\Sigma_{L/V}$.

2.2. **Energy and dissipation distance.** The relevant free energy is the capillary energy which consists of the energies of the three different interfaces. We consider this energy in nondimensional form, see the discussion in [1, Section 2(c)]. In this nondimensional formulation $\Sigma_{L/V}$ has energy per unit area equal to one. The liquid/solid interface has energy per unit area given by $-\cos\theta^Y$. Here θ^Y is the Young contact angle, i.e., the contact angle of a drop which minimizes the surface energy on a flat solid. Finally, the solid/vapour interface has zero energy. Thus, the energy of the system is given by

$$E\big(L\big) \;:=\; \big(|\Sigma_{S/L}|(-\cos\theta^Y) \,+\, |\Sigma_{L/V}|\big)\;, \tag{2.1}$$

where $|\Sigma|$ denotes the area of Σ. In the geometry of Figure 5, Equation (2.1) reads

$$E\big(L\big) \;=\; \big(|\Sigma_{S/L}|(-\cos\theta^Y) \,+\, |\Sigma_{L/V}\cap RS|\big) \,+\, \sqrt{1+\big(X(L)-Z(L)\big)^2}.$$

To introduce an external loading we force the upper interface point to move in time with unit speed. In fact, the choice of the velocity value is immaterial, because we are constructing a rate-independent model. The time dependent energy is then

$$E\big(t,L\big) \;:=\; \big(|\Sigma_{S/L}|(-\cos\theta^Y) \,+\, |\Sigma_{L/V}\cap RS|\big) \,+\, \sqrt{1+\big(X(L)\pm t\big)^2}.$$

We describe dissipation through the change in wetted solid area. This seems reasonable as it is well known that dissipation occurs mostly along the moving triple contact line. Thus, we define the energy dissipation in the time interval $[t_0,t_1]$ as

$$Diss\big(L,[t_0,t_1]\big) \;:=\; \int_{-R}^{R}\lambda\int_{t_0}^{t_1}\Big|\frac{d}{dt}\chi\big(L(t)\big)\Big|\,dtdS \tag{2.2}$$

where $\lambda\geq 0$ is a phenomenological material parameter and $\chi(L)$ is the characteristic function of L. The distance between two configurations is the minimal energy dissipated along a path joining them:

$$dist(L_0,L_1) := \inf_{L}\big\{Diss\big(L,[0,1]\big)\,\big|\,L(0)=L_0,\,L(1)=L_1\big\}.$$

The infimum is achieved for monotone L. Thus, the distance between two drops is the length of the solid wetted by only one of them:

$$dist(L_0, L_1) = \lambda \int_{-R}^{R} \big|\chi(L_1) - \chi(L_0)\big|\, dS. \tag{2.3}$$

This distance is macroscopically proportional to the usual distance between the two triple points. Notice, however, that the term dS in the last formula makes sure that only points belonging to the solid surface S contribute to this distance, with a weight decided by the phenomenological dissipation coefficient λ.

2.3. **Model for the stability of contact angles.** We look at a single drop L_0. To model the observed hysteresis we relax the condition that a stable drop is a local minimizer of the energy (leading to Young's law). Instead we only require L_0 to be stable in the following sense:

$$E(L_0) - E(\tilde{L}) \le dist(L_0, \tilde{L}) \tag{2.4}$$

for all $\tilde{L}$ which agree with L_0 on the upper boundary of B, i.e. on $\partial B \setminus \{[-R, R]\times 0\}$, but can have different contact angles. This is a global condition on the amount by which the energy can be reduced by changing L_0. Locally it says that the slope of the energy landscape at L_0 must not be too steep for L_0 to be stable. In fact, $E(L_0) - E(\tilde{L})$ has to fit under the cone $dist(L_0, \tilde{L})$, see Figure 6. It is crucial for *dist* to be homogeneous of degree one. This leaves some freedom for the slope at a stable point to be non zero. A quadratic polynomial for example can only lie above the energy at points with zero slope.

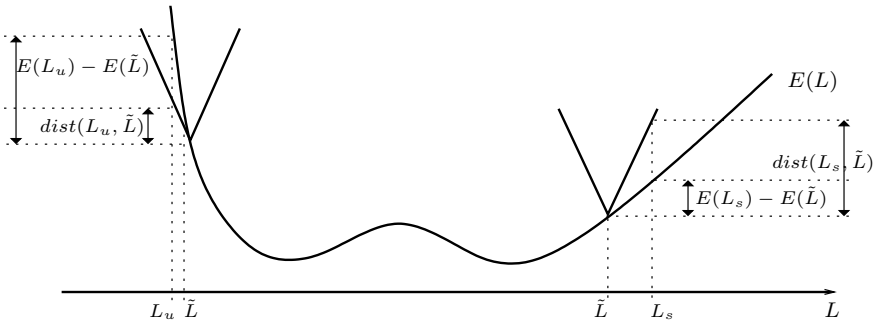

FIGURE 6. Energy landscape and dissipation distance

Furthermore, it is now clear that it suffices to consider drops whose liquid/vapour interfaces are straight lines. Drops with curved interfaces are unstable in the sense of (2.4) since straightening the interface reduces the energy without creating new distance.

2.4. **Model for quasistatic evolution.** External loading induces a change in the droplet configuration, as the energy becomes time dependent. This may lead to instabilities, and the system will jump to a new stable configuration. Following [13, Definition 2.1], we consider time evolutions L satisfying two conditions. First, at every time $t \in [0, \infty)$ the drop $L(t)$ has to be stable, i.e.:

$$E\big(t, L(t)\big) - E\big(t, \tilde{L}\big) \le dist\big(L(t), \tilde{L}\big) \tag{2.5}$$

for all $\tilde{L}$ which agree with $L(t)$ on the upper boundary of B.

Second, the dissipation must balance the energy difference together with the work done through the change in external loading:

$$E\big(t_1, L(t_1)\big) \,-\, E\big(t_0, L(t_0)\big) \,+\, Diss\big(L, [t_0, t_1]\big) \,=\, \int_{t_0}^{t_1} \partial_t E\big(s, L(s)\big)\, ds \qquad (2.6)$$

for all $t_0, t_1 \in [0, \infty)$, and for $Diss$ as defined in (2.2).

3. **Results.**

3.1. **Stable contact angles.** The model introduced in 2.3 gives four different diagrams for stable contact angles depending on the type of drop (Wenzel or Cassie–Baxter) and on the state of the surface on which it is resting (dry surface or surface with puddles). These diagrams (Figures 7–9) are plotted for the most interesting case, namely, under the assumption that $-\cos\theta^Y - \lambda < 0 < -\cos\theta^Y + \lambda$. We use the following notation

$$\begin{aligned} r^* &:= \frac{1-\varphi}{-\cos\theta^Y + \lambda} + \varphi, \\ r^{**} &:= \frac{1-\varphi}{\cos\theta^Y + \lambda} + \varphi, \end{aligned}$$

which gives $r^* < r^{**}$ for $-\cos\theta^Y > 0$ (the case shown below) and vice versa. Moreover, we write

$$\cos\theta^{CB} := -1 + \varphi + \varphi\cos\theta^Y\,. \qquad (3.1)$$

Figure 7 shows the negative cosines of the stable contact angles depending on the roughness r for the case of W–drops on a dry surface.

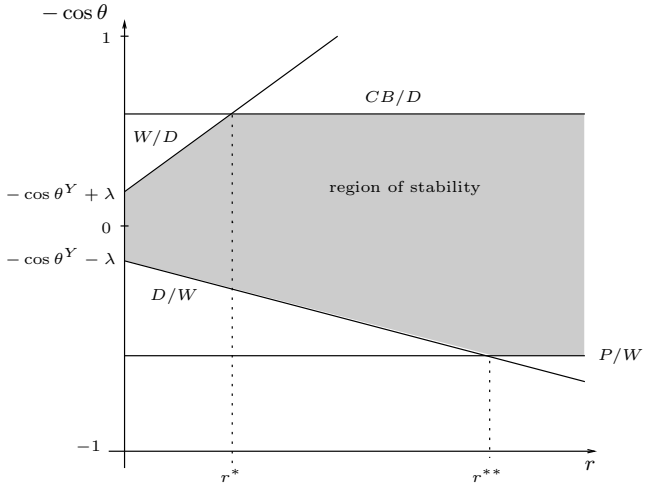

FIGURE 7. Stable contact angles for Wenzel drops on a dry surface

The region of stability is obtained from four bounds, which come from (2.4) by comparing with different types of test drops $\tilde{L}$. For the two upper boundaries, W/D and CB/D, the instability arises because the contact angle is too big. Therefore it is energetically advantageous to advance along the solid, i.e. the relevant comparison configurations $\tilde{L}$ in (2.4) are drops which have already advanced. The newly wetted area can have two different types of microstructure:

either W– or CB–type. Advancing with W–type microstructure gives instability if $-\cos\theta \geq W/D := r(-\cos\theta^Y + \lambda)$. Whereas advancing with CB–type implies instability if $-\cos\theta \geq CB/D := \varphi(-\cos\theta^Y + \lambda) + 1 - \varphi$. The two lower bounds, D/W and P/W, arise because the contact angle is too small. It is energetically better to recede from some area previously wetted. There are two possibilities to dewet area. Either the surface left behind is dry (D/W) or there are puddles on it (P/W). This gives instability if $-\cos\theta \leq D/W := r(-\cos\theta^Y - \lambda)$ and $-\cos\theta \leq P/W := \varphi(-\cos\theta^Y - \lambda) - 1 + \varphi$.

Summarizing, the hysteresis interval for a Wenzel drop on a dry surface is given by

$$-\cos\theta \in \begin{cases} \big(r(-\cos\theta^Y - \lambda)\,, r(-\cos\theta^Y + \lambda)\big) & \text{if } r \leq r^*\,, \\ \big(r(-\cos\theta^Y - \lambda)\,, -\cos\theta^{CB} + \lambda\varphi\big) & \text{if } r^* \leq r \leq r^{**}\,, \\ \big(-1 + \varphi + \varphi(-\cos\theta^Y - \lambda)\,, -\cos\theta^{CB} + \lambda\varphi\big) & \text{if } r^{**} \leq r\,, \end{cases} \tag{3.2}$$

where we recall that $-\cos\theta^{CB} = 1 - \varphi - \varphi\cos\theta^Y$, see (3.1). Notice that (3.2) provides λ with a physical interpretation, namely, that of half the hysteresis interval for an ideally flat ($r = 1$) surface.

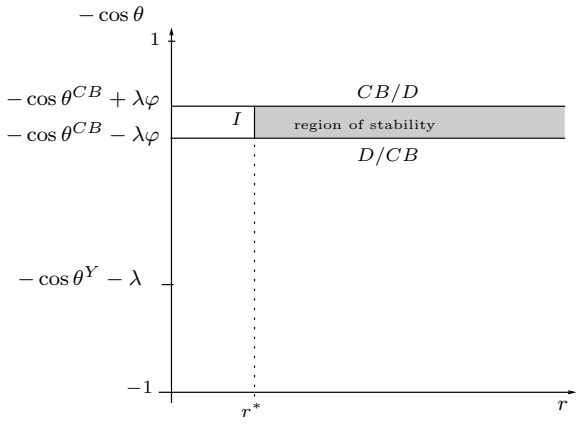

FIGURE 8. Stable contact angles for Cassie–Baxter drops on a dry surface

Our model implies a different diagram for CB–drops on a dry surface, see Figure 8. The advancing (upper) bounds are the same as for W–drops, as the microstructure under the drop does not play a role for advancing variations. The bound for advancing with W–type microstructure is not relevant as we get a new bound I which comes from interior variations. That is, we compare the drop L_0 of CB–type with a drop $\tilde{L}$ which wets the cavities underneath L_0, and obtain that CB–drops are never stable for $r < r^*$. For receding variations it is only relevant to recede with a dry surface. We get instability if $-\cos\theta \leq D/CB := \varphi(-\cos\theta^Y - \lambda) + 1 - \varphi$.

Summarizing, the hysteresis interval for a Cassie–Baxter drop on a dry surface is given by

$$-\cos\theta \in \big(-\cos\theta^{CB} - \lambda\varphi\,, -\cos\theta^{CB} + \lambda\varphi\big) \quad \text{for } r \geq r^*, \tag{3.3}$$

which gives a narrower hysteresis interval than for the flat surface, because $2\lambda\varphi < 2\lambda$. Notice that (3.3) predicts a linear dependence of the hysteresis interval on the areal density φ of solid tops. In the limit $\varphi \to 1$ we have $r^* \to 1$ and the hysteresis

interval tends to $(-\cos\theta^Y-\lambda, -\cos\theta^Y+\lambda)$ which is the interval for the flat surface ($r=1$). On the other hand in the limit $\varphi\to 0$ of small areal density of solid tops, $-\cos\theta^{CB}\to 1$ and the width of the hysteresis interval tends to zero. The material behaves ultra-hydrophobically. Notice that Diagram 8 and Equation (3.3) are valid independent of the sign of $\cos\theta^Y$ (hydrophobic or hydrophilic material).

We now turn to drops on a surface with puddles. Figure 9 shows the stable contact angles for W–drops on such a surface.

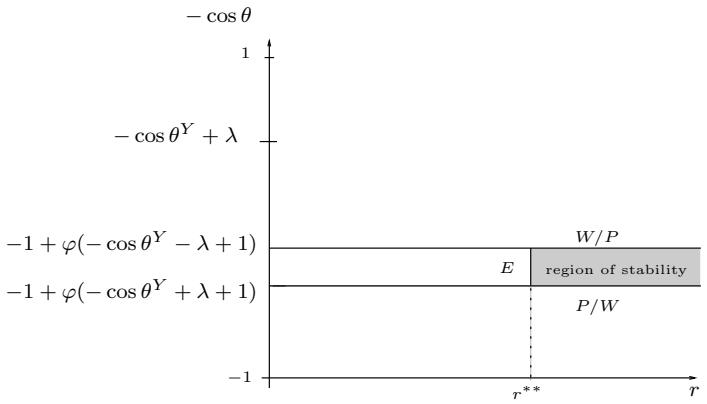

FIGURE 9. Stable contact angles for Wenzel drops on a surface with puddles

The bound $W/P := \varphi(-\cos\theta^Y+\lambda)-1+\varphi$ comes from advancing with W–type microstructure. For receding from wetted area we get the same bounds as for the dry surface because the surface structure is unimportant for receding from wetted area. The bound D/W does not play any role since there exist destabilizing exterior variations E (i.e., removing one of the puddles on the surface) which imply that puddles on a surface are instable for $r<r^{**}$.

Summarizing, the hysteresis interval for a Wenzel drop on a surface with puddles is given by

$$-\cos\theta\in\left(-1+\varphi(-\cos\theta^Y-\lambda+1)\,,-1+\varphi(-\cos\theta^Y+\lambda+1)\right)\quad\text{for } r\geq r^{**}\,. \tag{3.4}$$

CB–drops on a surface with puddles are never stable because they have the advancing bounds as for W–type on a surface with puddles, i.e. $W/P=\varphi(-\cos\theta^Y+\lambda)-1+\varphi$. On the other hand the receding bound is as for CB–drops on a dry surface, i.e. $D/CB=\varphi(-\cos\theta^Y-\lambda)+1-\varphi>W/P$.

The diagrams in Figures 7–9 are plotted under the assumption $-\cos\theta^Y-\lambda<0<-\cos\theta^Y+\lambda$, for which λ can be adjusted. Notice that they show the hydrophobic case, namely, $-\cos\theta^Y>0$. The same diagrams hold for a hydrophilic material but with $r^*>r^{**}$. In the case $-\cos\theta^Y-\lambda>0$, W–drops become unstable for $r>\frac{\varphi-1}{\cos\theta^Y+\lambda}+\varphi$ and puddles on the surface are never stable. For $-\cos\theta^Y+\lambda<0$, CB–drops are never stable.

3.2. **Quasistatic evolution.** Our model describes the time evolution of a drop driven by some external force. This force is represented by moving the upper interface point in time, see Section 2.2. The system responds in two steps. First the contact angle changes, with no motion of the contact line as long as the contact angles satisfy criterion (2.5). Then the triple point jumps to the next cavity. Hereby

it exhibits the microstructure with respect to which the contact angle became unstable. That is the microstructure which gives the relevant bound in Section 3.1.

Advancing and receding the drop more than once gives a hysteresis loop in the configurations of the drop and it finally leads to configurations that are stable with respect to further movements along the solid. The configurations shown in Figure 10 are the ones stable in this sense. To be more explicit: For fixed r, e.g. $r \in (r^*, r^{**})$ start with any kind of configuration, e.g. W–type on a dry surface. Then force the drop to recede. It will stay W leaving a dry surface behind. When forced to advance, however, the advancing front will turn to CB. If the whole drop starts moving, it will become a CB drop on a dry surface, and subsequent loading cycles will produce a stable (and smaller) hysteresis cycle with respect to the one exhibited during the first loading cycle.

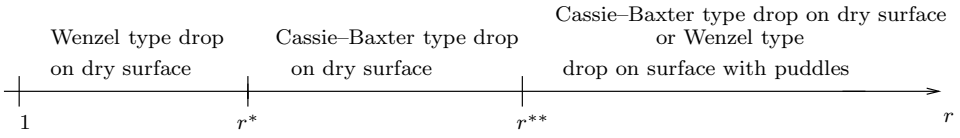

FIGURE 10. Stable configurations in the hydrophobic case

4. **Connection with experiments.** Figures 7 and 8 are in close qualitative agreement with the experiments in [11], which are done on a dry surface. The authors find a strong dependence of the stable contact angles on the type of drop: W–drops show a much stronger contact angle hysteresis than CB–drops, which is also predicted by our model. Figure 2 shows the separation of receding contact angles depending on the pressure pushing the drop onto the surface. The authors conjecture that high pressures induce W–drops, which have low receding contact angles. Whereas low pressures lead to CB–drops with high receding contact angles. Notice that the surface material used in [11] satisfies the condition valid for our diagrams, namely, $-\cos\theta^Y + \lambda > 0 > -\cos\theta^Y - \lambda$, which is that the receding (resp. advancing) contact angle for the flat surface are below (resp. above) 90°.

Our model sees the metastability of CB–drops pointed out in [11]. Here, as well as in the more recent studies [12] and [2], a transition from a CB–drop to a W–drop is observed, accompanied by a decrease in the contact angle. It is by now well known that the decrease of contact angle signals a transition from a higher to a lower energy state (see [16], [1]). Our model can reproduce this transition in so far as it allows for metastable drops. By defining $\bar{r}$ as the roughness where W and CB drops are of same energy, we get

$$\bar{r} := \frac{1-\varphi}{-\cos\theta^Y} + \varphi \; > \; r^*,$$

which leaves a range $(r^*, \bar{r})$ where CB drops are stable but do not minimize surface energy. Similarly for $r > \bar{r}$, W drops are stable in spite of their high surface energy.

The dependence of the stable contact angles on the drop type also explains the highly non–monotone behavior in Figure 1. The non–monotonicity comes from a jump in the type of drop. Figure 1 can be seen as a superposition of the diagrams in Figures 7 and 8. The choice of which diagram is valid can be done with the same arguments leading to Figure 10. For a dry surface the valid diagram changes at r^*, where we get a jump in the receding contact angle. This is because the

hysteresis interval for a CB–drop, the stable one for $r > r^*$, is much narrower than the hysteresis interval for a W–drop, the stable type for $r < r^*$.

Note that our model predicts a roughness–induced decrease of the receding contact angle for W–drops only in the case $-\cos\theta^Y - \lambda < 0$. This is not in agreement with the experiments in [7], which show a reduction of the receding contact angle with roughness also for surfaces which, when flat, exhibit contact angles slightly above 90°.

Our model can also reproduce the arguments in [10], that CB–drops can even be stable on a hydrophilic surface. Figure 8 is valid independent of the sign of $\cos\theta^Y$ hence, in particular, it applies to the hydrophilic case $\cos\theta^Y > 0$. The surface then behaves as ultra–hydrophobic for CB–drops with very little microscopic contact, since $-\cos\theta^{CB} := 1 - \varphi(1 + \cos\theta^Y) > 0$ for small φ, see Figure 11. Multiscale features in the surface roughness, suggested by the structure of some plants (see [3]), are sometimes invoked to explain this phenomenon (see [10]). However, hydrophobicity may come just as well from metastable configurations with very little contact with the surface, and it is possible to induce little contact through spikes standing far apart in the surface, without multiscale asperities.

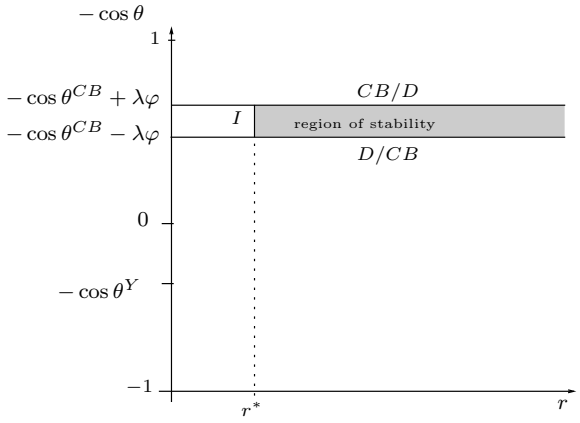

FIGURE 11. Stable Cassie–Baxter drops with ultrahydrophobic contact angles on a dry hydrophilic surface

5. **Proofs.**

5.1. **Stable contact angles.** We look at a fixed drop L_0. Without loss of generality assume $Z(L_0) = 0$. According to (2.4) we compare L_0 to all drops $\tilde{L}$ which agree with L_0 on the non–solid boundary of B. Rewrite (2.4) as

$$0 \le f_{L_0}(\tilde{L}, X(\tilde{L})) := E(\tilde{L}) - E(L_0) + dist(\tilde{L}, L_0)\,. \tag{5.1}$$

We consider drops $\tilde{L}$ whose microstructure agrees with L_0 inside its contact area but $\tilde{L}$ has advanced resp. receded. The area advanced resp. receded by $\tilde{L}$ contains many cavities as we are considering macroscopic variations. Therefore

$$f_{L_0}(\tilde{L}, X(\tilde{L})) = \big(X(\tilde{L}) - X(L_0)\big)\, C(L_0, \tilde{L}) + \sqrt{1 + (X(\tilde{L}))^2} - \sqrt{1 + (X(L_0))^2}\,,$$

where $C(L_0, \tilde{L})$ is the cost (i.e., the energy difference *plus* the dissipation distance) to pay for one cavity. We estimate this cost by a suitable average, in the same

spirit of the homogenized surface tensions defined in [1], where the interfacial energy is evaluated rigorously by homogenization methods in the limit of small scale asperities.

Look at $C(L_0, \tilde{L})$ for advanced area. This does not depend on the drop type L_0 but on the surface (with or without puddles) and the microstructure of $\tilde{L}$ on the advanced area. There is the possibility to advance with:

1. W–type on a dry surface: $C(L_0, \tilde{L}) = r(-\cos\theta^Y + \lambda) = W/D$
2. CB–type on a dry surface: $C(L_0, \tilde{L}) = \varphi(-\cos\theta^Y + \lambda) + 1 - \varphi = CB/D$
3. W–type on a surface with puddles: $C(L_0, \tilde{L}) = -1 + \varphi + \varphi(-\cos\theta^Y + \lambda) = W/P$.

Similarly the cost for a receded area does not depend on the surface type but on the microstructure of L_0 and the surface that is left behind:

1. W–type leave behind a dry surface: $C(L_0, \tilde{L}) = r(-\cos\theta^Y - \lambda) = D/W$
2. CB–type leave behind a dry surface: $C(L_0, \tilde{L}) = \varphi(-\cos\theta^Y - \lambda) + 1 - \varphi = D/CB$
3. W–type leave puddles behind: $C(L_0, \tilde{L}) = -1 + \varphi + \varphi(-\cos\theta^Y - \lambda) = P/W$
4. CB–type leave liquid tops behind: $C(L_0, \tilde{L}) = 1 - 2\varphi$.

These costs are the bounds for the cosines of the stable contact angles. To see this note that $f_{L_0}(L_0, X(L_0)) = 0$. We show that this is not a local minimum of f_{L_0}, if $-\cos\theta(L_0)$ is above resp. below $C(L_0, \tilde{L})$. This implies instability by (2.4) and (5.1).

$$\frac{d}{dX(\tilde{L})} f_{L_0}(\tilde{L}, X(\tilde{L})) \;=\; C(L_0, \tilde{L}) \;+\; \frac{X(\tilde{L})}{\sqrt{1 + (X(\tilde{L}))^2}} \;=\; C(L_0, \tilde{L}) \;+ \cos\theta(\tilde{L}).$$

But f_{L_0} has no local minimum at L_0 if the derivative for $X(\tilde{L}) > X(L_0)$, i.e. for advancing variations, is negative. Since we take the derivative at position $X(L_0)$ it is negative for one of the microstructures if $-\cos\theta(L_0) > \min\{C(L_0, \tilde{L})\}$. Analogously, L_0 is unstable with respect to receding variations if $-\cos\theta(L_0) < \max\{C(L_0, \tilde{L})\}$. This gives the bounds on the regions of stability in Section 3.1. Note that the receding bound for CB–drops which leave liquid tops behind (these configurations were suggested in [18]) is not relevant in our model because

$$\max\{1 - \varphi - \varphi(\cos\theta^Y + \lambda)\,,\, 1 - 2\varphi\} \;=\; 1 - \varphi - \varphi(\cos\theta^Y + \lambda).$$

The vertical bounds I and E in Section 3.1 come from interior and exterior variations. This means that we compare the drop L_0 with a drop $\tilde{L}$ having the same contact angle and microstructure as L_0 but one of the cavities interior or exterior to the contact area filled with vapor or liquid different from L_0. For example, for the I bound, the stability criterion (2.4) (applied to a cavity L_0 filled with vapor, which is compared to a water-filled cavity $\tilde{L}$) reduces to

$$\begin{aligned} 0 \;&\leq\; E(\tilde{L}) - E(L_0) + \mathit{dist}(\tilde{L}, L_0) \\ &=\; -r\cos\theta^Y - \left(1 - \varphi - \cos\theta^Y \varphi\right) + \lambda(r - \varphi)\,. \end{aligned}$$

This is satisfied if and only if

$$r \geq \frac{1 - \varphi}{-\cos\theta^Y + \lambda} + \varphi = r^*\,.$$

The argument for the E bound is analogous, and it leads to the inequality $r \geq r^{**}$ involving the second critical roughness coefficient r^{**}.

5.2. **Quasistatic evolution.** To prove that the time evolution described in 3.2 is consistent with our model we have to check (2.5) and (2.6).

Condition (2.5) is satisfied by construction. As long as the triple point does not move no energy is dissipated, therefore $Diss(L,[t_0,t))=0$. This turns (2.6) into:

$$E\big(t,L(t)\big)\;-\;E\big(t_0,L(t_0)\big)\;=\;\int_{t_0}^{t}\partial_t E\big(s,L(s)\big)ds,$$

which is satisfied as E is t-differentiable. Now look at a jump, and let t^* be the jump time. At t^* equation (2.6) turns into

$$E\big(t^*,L(t^*+)\big)\;-\;E\big(t^*,L(t^*-)\big)\;+\;Diss(L,[t^*,t^*])\;=\;0. \tag{5.2}$$

By definition,

$$Diss(L,[t^*,t^*])\;=\;dist\big(L(t^*+),L(t^*-)\big).$$

Therefore (5.2) is nothing but (2.5) written with equality, which is satisfied at the boundaries of the stability region. Here $L(t^*+)$ has the microstructure of $\tilde{L}$ with respect to which $L(t^*-)$ became unstable. Finally, notice that (2.6) is an additive equation.

Acknowledgements. We thank Martin Rumpf and Julia Dohmen for valuable discussions. This work was supported by the BMBF Förderbereich Mathematik and by INdAM "F. Severi" through the research project "Mathematical Challenges in Nanomechanics".

REFERENCES

[1] Alberti, G., DeSimone, A., *Wetting of rough surfaces: a homogenization approach*, Proc. R. Soc. London Ser. A Math. Phys. Eng. Sci., **461** (2005), 79–97.
[2] Bartolo, D., Bouamrirene, F., Verneuil, A., Buguin, A., Silberzan, P., Moulinet, S., *Bouncing or sricky droplets: Impalement transitions on superhydrophobic micropatterned surfaces*, Europhys. Letters **74** (2006), 299–305.
[3] Barthlott, W., Neinhuis, C., *Characterization and Distribution of Water–repellent, Self–cleaning Plant Surfaces*, Annals of Botany, **79** (1997), 667–677.
[4] Dal Maso, G., DeSimone, A., Mora, M.G., *Quasistatic evolution problems for linearly elastic–perfectly plastic materials*, Arch. Rat. Mech. Anal. **180** (2006), 237–291.
[5] de Gennes, P.G., *Wetting: statics and dynamics*, Rev. of Mod. Physics, **57** (1985), Part I, 827–863.
[6] de Gennes, P.G., Brochard-Wyart, F., Quéré, D., "Capillarity and Wetting Phenomena," Springer, 2004.
[7] Dettre, R.H., Johnson, R.E., *Contact Angle Hysteresis II. Contact Angle Measurements on Rough Surfaces*, Contact Angle, Wettability and Adhesion, Advances in Chemistry Series, **43** (1964), 136–144.
[8] Francfort, G., Marigo, J.J., *Revisiting brittle fracture as an energy minimization problem*, J. Mech. Phys. Solids, **50** (1998), 1319–1342.
[9] Francfort, G., Garroni, A., *A variational view of partial brittle damage*, Arch. Rat. Mech. Anal., **182** (2006), 125–152.
[10] Herminghaus, S., *Roughness–induced non–wetting*, Europhys. Letters, **52** (2000), 165–170.
[11] Lafuma, A., Quéré, D., *Superhydrophobic States*, Nature Materials, **2** (2003), 457–460.
[12] McHale, G., Aqil, S., Shirtcliffe, N.J., Newton, M.I., Erbil, H.Y., *Analysis of evaporation on a superhydrophobic surface*, Langmuir **21** (2005), 11053–11060.
[13] Mainik, A., Mielke, M., *Existence results for energetic models for rate–independent systems*, Calc.Var. **22** (2005), 73–99.
[14] Mielke, M., *Evolution of rate–independent systems*, Handbook of Differential Equations. Evolutionary Equations, vol. **2** (2005), 461–559.
[15] Mielke, M., Theil, F. *On rate independent hysteresis models*, NoDEA **11** (2004), 151–189.
[16] Patankar, N., *On the Modeling of Hydrophobic Contact Angles on Rough Surfaces*, Langmuir **19** (2003), 1249–1253.

[17] Quéré, D., *Rough ideas on wetting*, Physica A, **313** (2002), 32–46.
[18] Roura, P., Fort, J., *Comment on "Effects of the Surface Roughness on Sliding Angles of Water Droplets on Superhydrophobic Surfaces"*, Langmuir, **18** (2003), 566–569.

Received July 2006; revised January 2007.

E-mail address: desimone@sissa.it
E-mail address: grunewald@iam.uni-bonn.de
E-mail address: otto@iam.uni-bonn.de